Journal of Biomedical Optics 9(1), 121–125 (January/February 2004)

In vivo birefringence and thickness measurements of the human retinal nerve fiber layer using polarization-sensitive optical coherence tomography

Barry Cense
Harvard Medical School and
Wellman Laboratories of Photomedicine
Massachusetts General Hospital
50 Blossom Street BAR 714
Boston, MA 02114
E-mail: bcense@helix.mgh.harvard.edu

Teresa C. Chen
Harvard Medical School
Massachusetts Eye and Ear Infirmary
243 Charles Street
Boston, MA 02114

B. Hyle Park
Mark C. Pierce
Johannes F. de Boer
Harvard Medical School and
Wellman Laboratories of Photomedicine
Massachusetts General Hospital
50 Blossom Street
Boston, MA 02114
E-mail: deboer@helix.mgh.harvard.edu

Abstract. Glaucoma causes damage of the nerve fiber layer, which may cause loss of retinal birefringence. Therefore, PS-OCT is a potentially useful technique for the early detection of glaucoma. We built a fiber-based PS-OCT setup that produces real-time images of the human retina *in vivo*, coregistered with retinal video images of the location of PS-OCT scans. Preliminary measurements of a healthy volunteer show that the double-pass phase retardation per unit of depth of the RNFL is not constant and varies with location, with values between 0.18 and 0.37 deg/μm. A trend in the preliminary measurements shows that the nerve fiber layer located inferior and superior to the optic nerve head is more birefringent than the thinner layer of nerve fiber tissue in the temporal and nasal regions. [DOI: 10.1117/1.1627774]

Keywords: birefringence; glaucoma; retinal nerve fiber layer; polarization-sensitive optical coherence tomography.

Paper 103006 received Mar. 5, 2003; revised manuscript received Jun. 30, 2003; accepted for publication Jul. 1, 2003.

1 Introduction

Glaucoma is the world's second leading cause of blindness, causing damage to the retinal ganglion cells and thinning of the retinal nerve fiber layer (RNFL). When glaucoma is detected at an early stage, further loss of vision can be prevented by medication or surgery. Currently, there is no direct method that can measure the health and function of the RNFL. The visual field test is the current standard method of subjectively detecting loss of peripheral vision from glaucoma. However, up to 40% of the nerves can be irreversibly damaged before a clinically detectable loss of peripheral vision occurs.[1] There is therefore a need for objective instruments that can detect thinning of the nerve fiber layer before loss of vision.

Two such instruments that are in development are optical coherence tomography (OCT) and scanning laser polarimetry (SLP). With OCT, cross-sectional structural images of the retina can be made *in vivo*, allowing determination of the thickness of the RNFL.[2,3] Using light that is reflected back from the retina, SLP measures changes in polarization state, which are attributed to the birefringence of the RNFL.[4] Polarization-sensitive optical coherence tomography (PS-OCT) combines the depth resolution of OCT with the polarization sensitivity of SLP to obtain depth-resolved images of the optical birefringence of biological tissue.[5–10] *Ex vivo* measurements of primate and enucleated rabbit eyes demonstrated birefringence in the retinal nerve fiber layer and showed good correlation between the thickness determined with PS-OCT and histology.[11,12] Huang and Knighton[13] measured the single-pass phase retardation of isolated rat RNFL. Measurement of RNFL optical birefringence will enhance specificity in determining its thickness in structural OCT images. Although speculative, a decrease in birefringence could be an early sign of glaucomatous atrophy of the RNFL. We reported the first *in vivo* human depth-resolved measurements of RNFL birefringence.[10] Here we report measurements at six different locations around the optic nerve head (ONH) with the current setup.

2 Materials and Methods

In order to measure the RNFL birefringence in human subjects *in vivo*, we built a fiber-based PS-OCT setup that produces real-time images of the retina. In previous open-air PS-OCT systems, the tissue was usually probed with circularly polarized light.[5,6] A circularly polarized incident state is preferred, since it will always interact with birefringent tissue that has an optic axis in a plane perpendicular to the propagation direction of the beam. The polarization state of reflected light was compared with the incident circular state in order to determine the depth-resolved phase retardation. Compared to open-air systems, it is easier to construct a human eye measurement interface for fiber-based PS-OCT systems. However, in a fiber-based PS-OCT system, it is difficult to maintain a circular polarization state at the sample surface, since stress in the fibers and a noncircular shape of the fiber core will change the polarization state of the light traveling through the fiber. In previous fiber-based PS-OCT systems, this problem was overcome by a relative measurement method in which the tissue was probed with four or two different polarization states.[7–10]

1083-3668/2004/$15.00

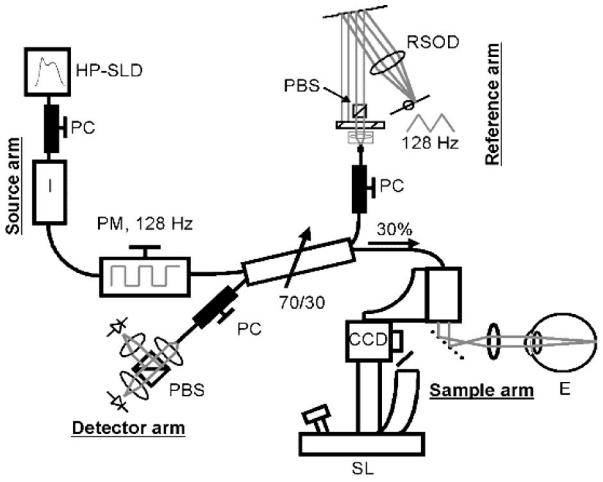

Fig. 1 Schematic overview of the fiber-based PS-OCT setup. Near-infrared light from a high-power superluminescent diode (HP-SLD) is sent through an isolator (I), after which it is polarization modulated (PM) and split by means of a 70/30 fiber coupler. Seventy percent of the light is injected into the rapid scanning optical delay line (RSOD), where a polarizer (PBS) ensures that light is always in the same linear state, regardless of changes in the polarization state in the fiber before the RSOD. Thirty percent of the power is directed toward the slit lamp (SL) in the sample arm. Light reflected back from the sample arm and delay line interferes in the detection arm and is split by a polarizing beamsplitter (PBS), after which both orthogonal states are detected by means of two silicon detectors.

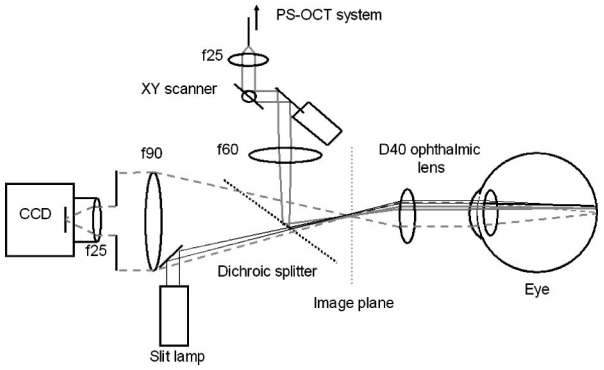

Fig. 2 Schematic overview of the optical paths in the slit lamp. A single-mode fiber guides the OCT beam into an XY galvanometer scanner. The f60 lens ($f=60$ mm), positioned 60 mm from the XY galvanometer scanner in the pupil plane, focuses the PS-OCT beam in the image plane. The ophthalmic D40 lens images the PS-OCT spot of the image plane onto the retina. During scanning, the sample beam pivots in the pupil plane positioned near the corneal surface. The retina is illuminated by the incoherent source of the slit lamp. The ophthalmic lens forms an image of the retina in the image plane, which is projected on the CCD chip through a dichroic splitter, transparent for visible light and highly reflective for near-infrared light. To avoid specular reflections that decrease the quality of recorded video images, the OCT beam and the illumination beam propagate off-axis through the D40 ophthalmic lens.

Here we have used two different polarization states, 90 deg apart on the Poincaré sphere, and generated by means of a piezodriven polarization modulator in the source arm. A high-power superluminescent diode (Superlum Russia) generated a broadband spectrum with a power of 4.6 mW (after polarization) and with a full width at half maximum (FWHM) bandwidth of 50 nm centered at 839 nm. The coherence function was measured on a mirror in water ($n=1.33$), giving an FWHM coherence length of 5.9 μm. In the retina, the axial resolution becomes 5.7 μm, assuming an index of refraction of 1.38. As shown in Fig. 1, a fiber coupler divided the light between sample and reference arms. The beamsplitter ratio in the interferometer was chosen as 70/30, since the power that can be sent into the eye has to be below the ANSI standard limit of 610 μW.[14] The sample arm consisted of a telecentric XY retina scanner and a headrest from a standard slit lamp, with the sample beam pivoting about the center of the entrance pupil of the eye (Fig. 2). Because aberrations are incurred in the cornea and lens, the optimal spot size (and therefore maximum retinal reflection) is obtained when the beam has a width of about 2 to 3 mm at the pupil plane.[15] A dichroic beamsplitter was used to reflect the sample beam toward a D40 ophthalmic Volk lens positioned 25 mm in front of the cornea. Incident power on the eye was 500 ± 5 μW, which is well below the maximum level specified in the ANSI standards. The retina was illuminated with an incandescent source of a slit lamp through the dichroic beamsplitter. Both the PS-OCT beam and the illumination beam traveled off-axis through the Volk lens to avoid the strong surface reflections from this lens and the cornea.

A charge-coupled device (CCD) camera was available for visual inspection of the retina and localization of PS-OCT scans in the retina. During a PS-OCT B-scan eight CCD images were acquired and stored on a hard disk. While 30% of the power was sent to the sample, the remaining 70% was directed toward the reference arm, which consisted of a rapid scanning optical delay line (RSOD).[16] A polarizing beamsplitter was used as a polarizer in order to ensure that the light in the RSOD was always in the same linear state, regardless of changes in the polarization state in the fiber before the RSOD. A polarization controller before the RSOD was aligned so that the power reflected from the RSOD was constant for both input polarization states. The dispersion in the sample and reference arms was matched by adjusting the grating to the lens distance in the delay line. The delay line's scanning mirror was positioned off-axis and driven by a triangular wave form with a frequency of 128 Hz synchronized with the polarization modulator, which was driven by a block wave of the same frequency. The carrier signal was at approximately 330 kHz and signals were digitally bandpass filtered with a bandwidth of 120 kHz centered at the carrier frequency.

Owing to the enhanced splitter ratio, 70% of the returned light from the sample arm went to the detection arm, while 30% of the light returning from the RSOD reached the detectors. The detection arm consisted of a polarization controller and a polarizing beamsplitter that split the light into two orthogonal components before detection by two silicon detectors. Signal detection was shot noise limited. The two signals were digitized with a 12-bit 2.5-MHz analog to digital (A/D) board and immediately stored on a hard disk. During one B-scan, 512 A-lines of 8192 samples to a depth of 1 mm in tissue were acquired in 2 s.

The accuracy of the phase retardation measurement was determined by measuring a calibrated mica wave plate with 58.6 deg single-pass retardance. Since the setup was designed

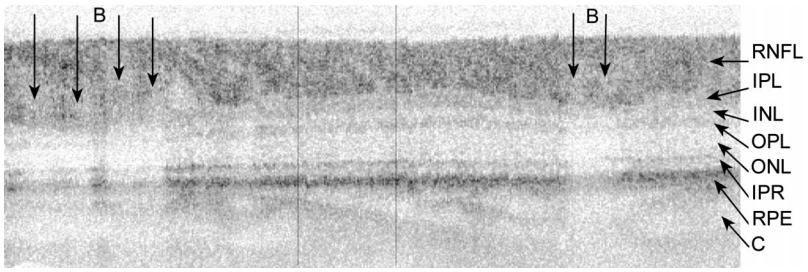

Fig. 3 Realigned intensity image of an area superior to the optic nerve head. The image is 2.1 mm wide by 0.7 mm deep. The dark top layer is the retinal nerve fiber layer (RNFL), followed by the inner plexiform layer (IPL), the inner nuclear layer (INL), the outer plexiform layer (OPL) and the outer nuclear layer (ONL). The two dark bands at the bottom of the image are the interface between the inner and outer segments of the photoreceptor layer (IPR) and the retinal pigmented epithelium (RPE). The structure below the RPE consists of choriocapillaris and choroid (C). The position of blood vessels can be recognized by a lower reflection signal below the vessels, owing to absorption in the blood. The blood vessels (B) are marked with vertical arrows. Double-pass phase retardation (DPPR) calculations were performed on regions of 64 averaged A-lines. An example of such a region is indicated by the two vertical lines.

to measure samples in a human eye through the cornea and lens, the setup had to be adapted for this calibration. An image of the wave plate was created in the image plane (see Fig. 2) by shifting the ophthalmic lens and increasing the length of the delay line. The wave plate was slightly tilted so that a small amount of light was reflected back into the PS-OCT system. Data were taken at two different optic axis orientations of the wave plate that were 90 deg apart.

All human experiments were performed under a protocol approved by the institutional review boards of both the Massachusetts Eye and Ear Infirmary and the Massachusetts General Hospital. The experiments were performed on a healthy 38-year-old-adult who had given informed consent. Prior to the measurements, the volunteer's right eye was dilated with a solution of 5.0% phenylephrine hydrochloride and 0.8% tropicamide. The images were taken superior, inferior, temporal, and nasal to the optic nerve head.

3 Results

By processing the interference fringe data as described earlier,[6–8] the 8192 samples within one A-line were converted to 1024 Stokes parameters I, Q, U, and V. An intensity image therefore consisted of 512 A-lines of 1024 pixels each, showing the intensity I gray scale encoded on a logarithmic scale over a dynamic range of 37 dB. White pixels represent areas with low reflection, while highly reflective areas are represented by black pixels. Figure 3 presents an intensity image recorded in an area superior to the optic nerve head. The image was realigned to remove axial motion artifacts. Structural features of the different layers in the retina are evident. Based on the work done by Drexler et al.,[3] subsequent layers can be identified as follows: The dark top layer is the highly scattering RNFL. At this retinal location, the thin ganglion cell layer located below the RNFL is difficult to identify. Below the RNFL we find the less scattering inner plexiform layer (IPL), the nearly transparent inner nuclear layer (INL), the scattering outer plexiform layer (OPL) and the nearly transparent outer nuclear layer (ONL). Both nuclear layers can be identified by a low reflectivity. The two dark bands below the ONL are the interface between inner and outer segments of the photoreceptor layer (IPR) and the retinal pigmented epithelium (RPE). The structure below the RPE consists of blood vessels in the choriocapillaris and choroid (C). The presence of blood vessels in the RNFL at the left and right side of the image is indicated by a reduced intensity reflected from the RPE below these structures, which is attributed to signal attenuation by blood absorption. The blood vessels are marked with arrows. Figure 4 shows the location of individual scans superior to the ONH in the retina.

For double-pass phase retardation (DPPR) calculations, two adjacent A-lines, created with two different input polarization states, are necessary to calculate one DPPR A-line. In the phase retardation calculation, a considerable reduction of speckle noise was achieved by averaging the Stokes parameters of 32 adjacent A-lines with the same input polarization state. The surface Stokes vector was calculated 10 μm below the surface edge, which was determined from the I Stokes parameter in an A-line by a threshold function, preceded by a 3×3 median filter. Stokes vectors at the RNFL's surface were compared with Stokes vectors at lower depths to determine DPPR and optic axis orientation.[6–8] Figure 5 shows the evolution of the two incident Stokes states over the surface of the Poincaré sphere with increasing depth of tissue for the delineated region of 64 A-lines in Fig. 3. The rotation of both states over an arc around a single axis explicitly demonstrates birefringence with a single optic axis, as expected for the regularly oriented fibers in the RNFL. The angle between two equidistant Stokes vectors was approximately 90 deg on the Poincaré sphere. Analysis of the wave plate measurements

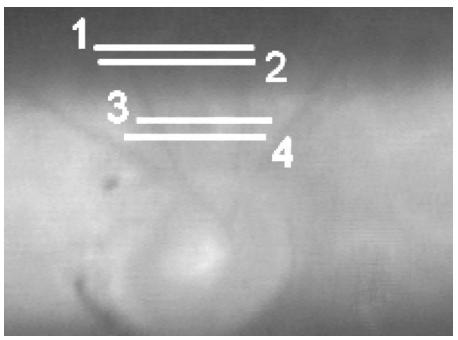

Fig. 4 CCD image of the retina, showing the position of individual scans superior to the optic nerve head (ONH). The intensity OCT image of scan 3 is shown in Fig. 3.

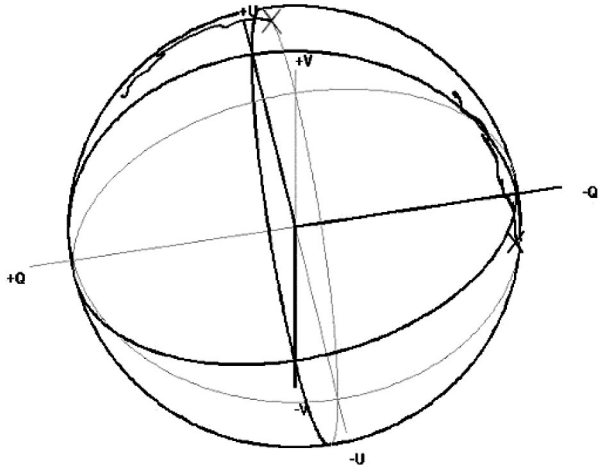

Fig. 5 Evolution of the two incident polarization states over the Poincaré sphere as a function of depth, using data averaged over 64 A-lines. The Poincaré sphere is oriented so that the axis of rotation is pointing out of the plane of the drawing. Thick lines on the sphere's surface show the change in Stokes vectors over a distance of 140 μm in the RNFL, and crosses indicate the surface Stokes states. The DPPR is derived from the angle of rotation about the optic axis, starting with the Stokes vector that belongs to the surface and finishing with the vector that belongs to a certain depth.

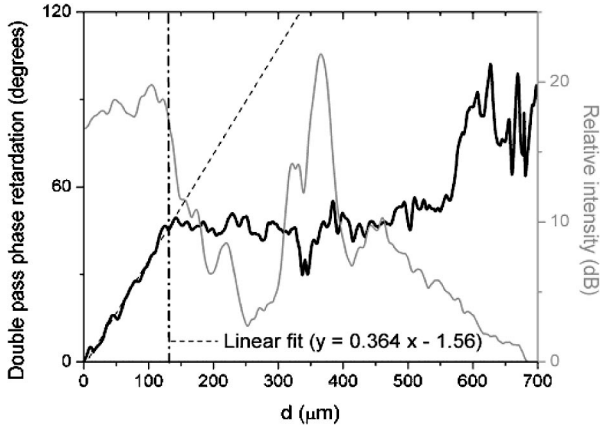

Fig. 6 Double-pass phase retardation as a function of depth, using the data from Fig. 3 and Fig. 5. Black line, double-pass phase retardation; gray line, reflected intensity; dashed line, least-squares linear fit to double-pass phase retardation data over a region considered to belong to the RNFL. The vertical dash-dot line represents the estimated RNFL boundary.

showed that the birefringence measurement was accurate within 3%, independent of the orientation of the optic axis of the wave plate.

Corneal birefringence changes the incident polarization state unpredictably.[17] Since the RNFL surface is used as a reference in the phase retardation calculation, our method is not influenced by corneal birefringence.

Images taken with the slit lamp's near-infrared-sensitive CCD camera were used to determine the location of a B-scan in the retina. The PS-OCT data were analyzed in order to quantify the birefringence of the RNFL and to determine a relationship between location in the RNFL and birefringence. In an image, the RNFL was divided into eight regions, each with 64 A-lines. The DPPR per unit of depth (DPPR/UD) of each region was calculated. Data points that were considered to originate from the RNFL were fitted with a linear least-squares fit, with the slope yielding the reported DPPR/UD. The corresponding intensity graph was used to determine the boundaries of the RNFL. Regions with visible blood vessels were excluded because the absence of birefringence in blood vessels distorted the birefringence measurement in nerve tissue.

As an example, Fig. 6 shows the DPPR, the reflected intensity, and a linear fit to the DPPR, which corresponds to the delineated area in Fig. 3 and data in Fig. 5. Both the intensity and phase retardation graphs were used to determine the position of the RNFL boundary, represented by the vertical dash-dot line. In the intensity graph, a sharp drop in intensity indicates the border between the RNFL and ganglion cell layer. In the DPPR graph, birefringence of RNFL tissue linearly increases the DPPR as a function of depth. Between the RNFL and the choroid, the DPPR is constant and indicates an absence of birefringence in the inner and outer plexiform layer, inner and outer nuclear layer, inner and outer segments of the photoreceptor layer, RPE, and choroid. The strong reflection from the RPE renders values that are equal to the values measured at the bottom of the RNFL, strongly supporting an absence of birefringence between the RNFL and the RPE. Therefore the transition from a linearly increasing value to a constant value in the DPPR graph indicates the RNFL boundary. Below the RPE, the intensity drops further while the double-pass phase retardation increases. This could indicate the presence of a highly birefringent medium like collagen in the sclera. An alternative explanation for the rise in DPPR values is that when the reflected signal at this depth is low, as can be seen in the intensity graph of Fig. 6, the DPPR increases to 115 deg.[8,10] This lower reflected signal is possibly caused by the attenuation of light in the blood vessels of the choroid above this layer.

In order to show the relationship between birefringence and the position in the retina, data were taken from six different regions and analyzed. These six regions were temporal, nasal, inferior, and superior to the optic nerve head, with locations close and far away from the optic nerve head in the inferior and superior regions. Only one area close to the optic nerve head was selected in the temporal and nasal regions. In the inferior and superior parts, the RNFL is relatively thick and changes in thickness as a function of the distance from the center of the optic nerve head. For instance, in Fig. 4, in scans 1 and 2, which are located approximately 1.2 mm from the center of the optic nerve head, the average RNFL thickness is 90 μm. In scans 3 and 4, located approximately 0.65 mm from the center of the optic nerve head, the nerve fiber thickness has increased to 150 μm. In Fig. 7, the relationship between RNFL averaged thickness, retinal location, and measured DPPR/UD is shown. The horizontal and vertical error bars indicate the standard deviations of RNFL thickness and DPPR/UD within an averaged area, respectively. The following trend is observed: Thicker nerve fiber layer tissue located in inferior and superior regions exhibits stronger birefringence than the thinner tissue located in the temporal and nasal regions. This difference might be caused by a difference in nerve fiber layers tissue birefringence as a function of location

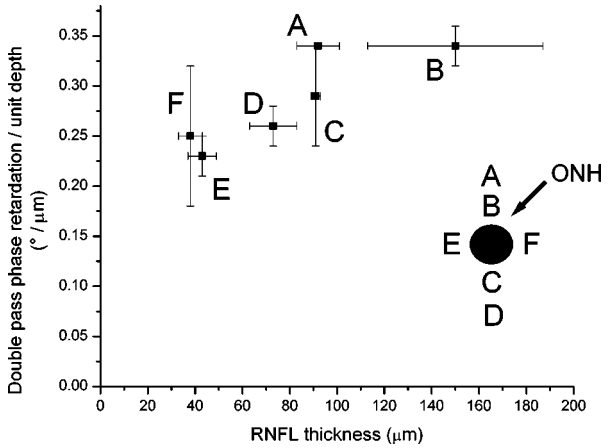

Fig. 7 The relationship between the thickness of the nerve fiber layer, the retinal location, and the measured DPPR. The letters in the drawing indicate the locations of averaged measurements around the ONH and correspond to the labeled values in the graph. The number of averaged points per area was as follows: A (n=15); B (n=13); C (n=15); D (n=16); E (n=16); F (n=16). The error bars indicate the standard deviation of the averaged thickness and DPPR per unit of depth (UD) values. The DPPR/UD values of this volunteer's RNFL vary between 0.18 and 0.37 deg/μm.

or by a difference in birefringence as a function of thickness. DPPR/UD values are not constant, but vary between 0.18 and 0.37 deg/μm.

4 Discussion

Ducros et al.[12] measured the DPPR/UD at a wavelength of 859 nm in the RNFLs of primates. They found a typical value of 0.29 deg/μm. Huang and Knighton[13] measured the single-pass phase retardation of isolated rat RNFL. At 830 nm and converting to double pass, they found average DPPR/UD values of 0.20 deg/μm. Both results are in good agreement with values reported here.

5 Conclusion

PS-OCT is a modality suitable for *in vivo* depth-resolved birefringence measurements in the human retina. Phase retardation measurements were accurate within 3%, independent of the orientation of the optic axis. Preliminary measurements on one volunteer show that the double-pass phase retardation in the RNFL near the optic nerve head is not constant, but varies between 0.18 and 0.37 deg/μm. The following trend was observed: Retinal nerve fiber layer tissue located inferior and superior to the optic nerve head is more birefringent than the thinner nerve fiber layer tissue in the temporal and nasal regions.

Acknowledgments

Research grants from the National Eye Institute (1R 24 EY 12877), Whitaker Foundation (26083), and a generous gift from Dr. and Mrs. J. S. Chen to the Optical Diagnostics Program of the Wellman Laboratories of Photomedicine are gratefully acknowledged for the support of this research.

References

1. H. A. Quigley, E. M. Addicks, and W. R. Green, ''Optic nerve damage in human glaucoma. III. Quantitative correlation of nerve fiber loss and visual field defect in glaucoma, ischemic neuropathy, papilledema, and toxic neuropathy,'' *Arch. Ophthalmol. (Chicago)* **100**, 135–146 (1982).
2. J. S. Schuman, M. R. Hee, C. A. Puliafito, C. Wong, T. Pedut-Kloizman, C. P. Lin, E. Hertzmark, J. A. Izatt, E. A. Swanson, and J. G. Fujimoto, ''Quantification of nerve fiber layer thickness in normal and glaucomatous eyes using optical coherence tomography,'' *Arch. Ophthalmol. (Chicago)* **113**(5), 586–596 (1995).
3. W. Drexler, H. Sattmann, B. Hermann, T. H. Ko, M. Stur, A. Unterhuber, C. Scholda, O. Findl, M. Wirtitsch, J. G. Fujimoto, and A. F. Fercher, ''Enhanced visualization of macular pathology with the use of ultrahigh-resolution optical coherence tomography,'' *Arch. Ophthalmol. (Chicago)* **121**, 695–706 (2003).
4. R. N. Weinreb, A. W. Dreher, A. Coleman, H. Quigley, B. Shaw, and K. Reiter, ''Histopathologic validation of Fourier-ellipsometry measurements of retinal nerve fiber layer thickness,'' *Arch. Ophthalmol. (Chicago)* **108**(4), 557–560 (1990).
5. J. F. de Boer, T. E. Milner, M. J. C. van Gemert, and J. S. Nelson, ''Two-dimensional birefringence imaging in biological tissue by polarization-sensitive optical coherence tomography,'' *Opt. Lett.* **22**(12), 934–936 (1997).
6. J. F. de Boer, T. E. Milner, and J. S. Nelson, ''Determination of the depth-resolved Stokes parameters of light backscattered from turbid media by use of polarization-sensitive optical coherence tomography,'' *Opt. Lett.* **24**(5), 300–302 (1999).
7. C. E. Saxer, J. F. de Boer, B. H. Park, Y. Zhao, Z. Chen, and J. S. Nelson, ''High-speed fiber-based polarization-sensitive optical coherence tomography of in vivo human skin,'' *Opt. Lett.* **25**(18), 1355–1357 (2000).
8. B. H. Park, C. E. Saxer, S. M. Srinivas, J. S. Nelson, and J. F. de Boer, ''In vivo burn depth determination by high-speed fiber-based polarization sensitive optical coherence tomography,'' *J. Biomed. Opt.* **6**(4), 474–479 (2001).
9. M. C. Pierce, B. H. Park, B. Cense, and J. F. de Boer, ''Simultaneous intensity, birefringence, and flow measurements with high-speed fiber-based optical coherence tomography,'' *Opt. Lett.* **27**(17), 1534–1536 (2002).
10. B. Cense, T. C. Chen, B. H. Park, M. C. Pierce, and J. F. de Boer, ''In vivo depth-resolved birefringence measurements of the human retinal nerve fiber layer by polarization-sensitive optical coherence tomography,'' *Opt. Lett.* **27**(18), 1610–1612 (2002).
11. M. G. Ducros, J. F. de Boer, H. E. Huang, L. C. Chao, Z. Chen, J. S. Nelson, T. E. Milner, and H. G. Rylander, ''Polarization-sensitive optical coherence tomography of the rabbit eye,'' *IEEE J. Sel. Top. Quantum Electron.* **5**(4), 1159–1167 (1999).
12. M. G. Ducros, J. D. Marsack, H. G. Rylander, S. L. Thomsen, and T. E. Milner, ''Primate retina imaging with polarization-sensitive optical coherence tomography,'' *J. Opt. Soc. Am. A* **18**(12), 2945–2956 (2001).
13. X. Huang and R. W. Knighton, ''Linear birefringence of the retinal nerve fiber layer measured in vitro with a multispectral imaging micropolarimeter,'' *J. Biomed. Opt.* **7**(2), 199–204 (2002).
14. American National Standards Institute, *Safe Use of lasers*, ANSI standard Z136.1, Laser Institute of America, Orlando, FL (1993).
15. F. W. Campbell and D. G. Green, ''Optical and retinal factors affecting visual resolution,'' *J. Physiol. (London)* **181**, 576–593 (1965).
16. G. J. Tearney, B. E. Bouma, and J. G. Fujimoto, ''High-speed phase- and group-delay scanning with a grating-based phase control delay line,'' *Opt. Lett.* **22**(23), 1811–1813 (1997).
17. D. S. Greenfield, R. W. Knigton, and X. Huang, ''Effect of corneal polarization axis on assessment of retinal nerve fiber layer thickness by scanning laser polarimetry,'' *Am. J. Ophthalmol.* **129**, 715–722 (2000).